Effects of a random porosity model on heat transfer performance of porous media

Wu-Shung Fu*, Hsin-Chien Huang

Department of Mechanical Engineering, National Chiao Tung University, Hsinchu, 30050, Taiwan, Republic of China

Abstract

Due to the non-uniform distribution and fractural structure of the beads inside a porous medium, the porosity distributed in the porous medium is random for most realistic situations. Therefore, the effects of the porosity distributed casually inside a porous block mounted on a heated region with a laminar slot impinging jet on flow and thermal fields are investigated numerically. A numerical method of SIMPLEC is adopted to solve governing equations, as for the energy equation, a one-equation thermal model with Van Driest's wall function is adopted. All the non-Darcian effects including the solid boundary and inertial effects are considered and three different porosity models of constant, variable and random are examined. The results indicate that the relationship between the local Nusselt number Nu_x and the near wall local porosity ε_x is a negative correlation. Consequently, in order to enhance the thermal performance of the porous medium, the porosity near the solid plate should be smaller to make the conductive heat transfer to be dominant. © 1998 Elsevier Science Ltd. All rights reserved.

Nomenclature

b width of the slot jet [m]
B_0 coefficient of stagnant conductivity
C_f specific heat of fluid [kJ kg^{-1} °C^{-1}]
d_p mean bead diameter [m]
Da Darcy number ($= K/b^2$)
D_T empirical constant in thermal dispersion conductivity
F inertial factor
h_x local heat transfer coefficient [W m^{-2} °C^{-1}]
H_j dimensional distance from the jet inlet to the top surface of the block [m]
H_p dimensional height of the block [m]
H_z dimensional distance from the jet inlet to the solid wall [m]
HJ dimensionless distance from the jet inlet to the top surface of the block ($= H_j/b$)
HP dimensionless height of the block ($= H_p/b$)
HZ dimensionless distance from the jet inlet to the solid wall ($= H_z/b$)

k_d stagnant conductivity [W m^{-1} °C^{-1}]
k_e effective thermal conductivity of the porous block [W m^{-1} °C^{-1}]
k_f thermal conductivity of the fluid [W m^{-1} °C^{-1}]
k_s thermal conductivity of solid phase in porous block [W m^{-1} °C^{-1}]
k_t thermal dispersion conductivity [W m^{-1} °C^{-1}]
K permeability [m^2]
l Van Driest's wall function
L_p dimensional length of the block [m]
LP dimensionless length of the block ($= L_p/b$)
$\dot{m}$ dimensionless flow rate of fluid
$N(a, b^2)$ normal distribution with mean a and standard deviation b
Nu_x local Nusselt number along the heated wall of the block ($= h_x b/k_f$)
$\overline{Nu}$ mean Nusselt number
p dimensional pressure [N m^{-2}]
P dimensionless pressure ($= p/\rho v_0^2$)
Pr_f Prandtl number of fluid ($= \rho_f C_f v_f/k_f$)
Pr_p Prandtl number of porous medium ($= \rho_f C_f v_f/k_e$)
r_1, r_2 coefficient in equation (2)
Re Reynolds number ($= v_0 b/v_f$)
Re_p bead diameter based Reynolds number ($= |\mathbf{u}_p|\overline{d_p}/v_f$)
T temperature [°C]

* Corresponding author. Tel.: 886 3 5712121; fax: 886 3 5720634

u dimensional velocity in the x direction [m s^{-1}]
U dimensionless velocity in the X direction ($=u/v_0$)
v dimensional velocity in the y direction [m s^{-1}]
v_0 jet inlet velocity [m s^{-1}]
V dimensional velocity in the Y direction ($=v/v_0$)
x, y dimensionless Cartesian coordinates [m]
X, Y dimensionless Cartesian coordinates ($=x/b$, $=y/b$).

Greek symbols
α thermal diffusivity [m^2 s^{-1}]
Δs shortest distance from the calculated point to the boundaries of the porous block
ε porosity
$\bar{\varepsilon}$ mean porosity
ε_e effective porosity
ε_x near wall local porosity at $Y = 0.0015$
θ dimensionless temperature ($=(T-T_0)/(T_w-T_0)$)
Λ ratio of thermal conductivity of solid phase to fluid phase in porous block
μ viscosity [kg m^{-1} s^{-1}]
v kinematic viscosity [m^2 s^{-1}]
ξ random variable
ρ fluid density [kg m^{-3}]
σ_ε standard deviation of porosity
Φ computational variable
ψ dimensionless stream function
ω empirical constant in Van Driest's wall function.

Superscripts
n the nth iteration index
—   mean value.

Subscripts
c.v.   control volume
e   effective value
f   external flow field
i   index
in   flowing into porous block
out   leaving from porous block
p   porous medium
s   solid block
w   solid wall
x along the X direction
0   inlet condition.

Other
| | magnitude of velocity vector.

1. Introduction

It is a well-known method that a metal porous block is adopted to disturb fluid flow and enlarge heat transfer surface which enhances heat transfer rate. The issue is studied widely and deeply in the last decade.

Doubtless, porosity is a remarkable factor during analyzing the fluid flow and heat transfer of porous medium. For facilitating analyses, in the beginning the porosity was usually assumed as a constant, which is conveniently called a constant porosity model in this study. However, Roblee et al. [1] and Benenati and Brosilow [2] based on their experimental results observed that porosity varied significantly in the near-wall region. Schwartz and co-workers [3, 4] conducted experimental studies and measured the maximum velocity in the near wall region which is normally called the channelling effect. These phenomena directly validated that the porosity which was regarded as a variable was more realistic. Furthermore, Cheng et al. [5] pointed out that in much of the literature the porosity was simulated as a damped oscillatory function of the distance from the wall and the damped oscillatory phenomenon was insignificant as the distance was larger than five-bead diameters for packed beds. Therefore, in concerning both of the practical use and convenient theoretic model, the variation of the porosity is assumed as an exponential function of the distance from the solid wall and is called a variable porosity model for comparing with the constant porosity model. Based upon the above experience, two different models have been adopted to derive the individual equations of fluid flow and heat transfer for the porous medium.

For the constant porosity model, Vafai and Tien [6] according to the concept of local volume averaging analysis derived the governing equations of fluid flow and heat transfer for the porous medium. As for the variable porosity model, Hsu and Cheng [7] utilized the volume averaging technology to derive the governing equations of the fluid flow and heat transfer for the porous medium. Both the above two different types of the governing equations were widely employed to study the effect of the inertia term, solid boundary and variable porosity on the fluid flow and heat transfer of the porous medium in both forced and natural convections, such as Vafai and co-workers [8, 9], Kaviany [10], Cheng and Zhu [11], Hadim [12], Hunt and Tien [13] and Fu and co-workers [14–16], etc.

However, Georgiadis and co-workers [17–19] studied the unidirectional transport phenomena of flow and heat transfer in the random porous medium with stochastic models and obtained the results that for the same pressure gradient along the channel the mean flow rate $\overline{U(\varepsilon)}$ based on random porosity was larger than $U(\bar{\varepsilon})$ based on mean porosity as the Forchheimer model of flow was held. Saito et al. [20] studied the effects of the porosity and void distributions on the permeability by using Direct Simulation Monte Carlo method and found that the permeability depended not only on the porosity but also on the void distribution strongly. These facts indicated that except for special screen process the sizes of the beads are extremely difficult to be uniform. Besides, the geometry of the broad definition of beads is not always spherical

and sometimes is fragmental. Therefore, the characteristics of the porosity distribution being disordered and random which results from the non-uniform size and fractural structure of the beads should be considered for a more realistic model of the porous medium. This model is abbreviated to the random porosity model. Although the effect of the random porosity distribution on the flow field had been discussed in the past, however, most of them were only concentrated on simple phenomena. As the knowledge of the authors, the results and discussion of the heat transfer and fluid flow mechanisms of the porous medium with the random porosity model were seldom presented in detail.

Consequently, the aim of this study is to investigate effects of a random porosity model on heat transfer performance of a porous block under an impinging jet numerically. The distribution of the porosity follows the normal (Gaussian) distribution rule and is generated by Kinderman–Ramage procedure [21]. The diameters of 101 beads of a porous block are measured to obtain a reasonable mean porosity and standard deviation of the porosity. The constant and variable porosity models are also considered. A numerical method of SIMPLEC [22] is adopted to solve the governing equations, as for the energy equation, a one-equation thermal model with Van Driest's wall function is adopted. All the non-Darcian effects including the solid boundary effects and inertial effects are considered. Other important parameters such as Reynolds number, geometry size ratios of the porous block and Prandtl number, etc., are selected based on the author's previous studies [14–16]. The results indicate that the relationship between the local Nusselt number Nu_x and the near wall local porosity ε_x is a negative correlation. Consequently, in order to enhance effectively the thermal performance of the porous medium, the porosity near the solid plate should be smaller to make the conductive heat transfer dominant.

2. Physical model

The physical model is shown symmetrically in Fig. 1. There is a two-dimensional laminar slot jet impinging on a partially heated plate. The width of the jet inlet is b. The uniform inlet velocity and temperature of the jet are v_0 and T_0, respectively. A portion of the impingement plate is heated and the other region is insulated. The length of the heated region is L_p, and the temperature of the heated region is T_w which is higher than T_0. A porous block of which the porosity distribution is corresponding to the random porosity model is mounted on the heated region. Based on the results of Fu and Huang [15, 16], the height H_p and the length L_p of the block are chosen to 0.5b and 2b, respectively. The distances from the jet inlet to the top surface of the block and the impingement plate are H_j ($=3.5b$) and H_z ($=4.0b$), respectively. The
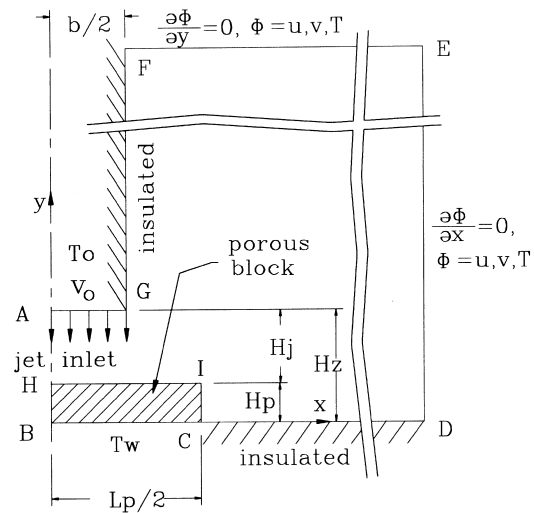
Fig. 1. Physical model.

whole computation domain is large enough for fully developed distributions of the velocity and temperature to be formed. Under this configuration, the flow field can be decomposed into two conjugate regions: one stands for the internal flow field where it is bounded by the porous block, and the other is called the external flow field which excludes the porous media.

In order to facilitate the problems, the following assumptions are made

(1) The porous block is made of copper beads which have different sizes of diameters. The beads do not chemically react with the fluids.
(2) The flow field is steady state, two-dimensional, single phase, laminar and incompressible. The symmetrical assumption shown in Fig. 1 exists in the random porosity model.
(3) The fluid properties are constant and the effect of gravity is neglected.
(4) The transverse thermal dispersion is modeled by Van Driest's wall function [23], hence, a one-equation model of the energy equation is used for the porous medium.
(5) The effective viscosity of the porous medium is equal to the viscosity of the external fluid.

As mentioned above, the values of the porosity distributed in the porous medium are random. Then the following process is used to obtain the data of the mean porosity $\bar{\varepsilon}$ and standard deviation σ_ε. The diameters of 101 beads are ensampled and measured from decomposition of a sintered brass porous block. The diameters are classified and shown in Fig. 2. The mean diameter $\bar{d}_p$ of the beads is about 1.35 mm and its standard deviation is 0.16 mm which is about 12% of the mean diameter of
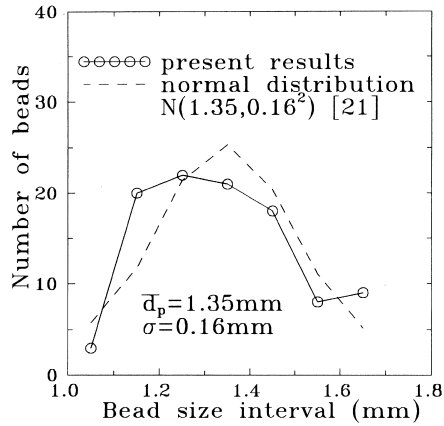
Fig. 2. The size distribution of 101 beads in a porous block.

the beads. Shown in Fig. 2, the distribution of the bead sizes is like a normal distribution. As a result, the space occupied by the solid phase in the porous medium is corresponding to the normal distribution. Then that the residual space (void phase) in the porous medium also follows the normal distribution rule can be drawn. Based on the data of the density of the beads provided by the bead maker, the maximum mean porosity of the porous block is approximately estimated as 0.47. Therefore, in this study, the mean porosity $\bar{\varepsilon}$ is conveniently regarded as 0.5 and the standard deviation σ_ε is 0.05 which is 10% of the mean porosity. The mean diameter $\overline{d}_p$ is selected as a characteristic bead diameter and equal to 1.25 mm for easily presenting the results.

In order to compare the difference among the models of constant porosity, variable porosity and random porosity, three models of porosity distribution are taken into consideration. They are

(1) constant porosity model: $\varepsilon = \bar{\varepsilon}$ (1)

(2) variable porosity model: $\varepsilon = \varepsilon_e[1 + r_1 e^{-r_2 \Delta s/\overline{d}_p}]$ (2)

where Δs is the shortest distance from the calculated point to the boundary of the porous block, and r_1 and r_2 are both empirical constants. The ε_e is an effective porosity. The mean porosity $\bar{\varepsilon}$ can be obtained from integrating the local porosity ε in the full domain of the porous block as follows

$$\bar{\varepsilon} = \frac{1}{L_p \times H_p} \int_0^{L_p} \int_0^{H_p} \varepsilon_e[1 + r_1 e^{-r_2 \Delta s/\overline{d}_p}]\, \mathrm{d}y\, \mathrm{d}x \quad (3)$$

where the r_2 is obtained from Vafai [8] and the r_1 is selected to make the local porosity in the near wall region to be equal to one. As a result, for the cases of $\bar{\varepsilon} = 0.5$, the ε_e, r_1 and r_2 are equal to 0.307, 2.256 and 2, respectively.

(3) Random porosity model: according to the results of the measuring process, the porosity distribution of the porous medium approximately follows the form of the

normal distribution with mean porosity $\bar{\varepsilon}$ and standard deviation σ_ε shown in Fig. 2. For necessity of computing process, the theoretic form of the porosity distribution of the random porosity model is obtained from the following method. The Kinderman–Ramage procedure [21] (Appendix) is used to generate a random variable ξ of the standard normal distribution, $N(0, 1)$, first. And the random variable ξ is transformed to gain a general random variable ε corresponding to a general normal distribution, $N(\bar{\varepsilon}, \sigma_\varepsilon^2)$, of which the mean $\bar{\varepsilon}$ and standard deviation σ_ε are equal to designed constants, respectively. Therefore, the distribution of the general random variable ε is regarded as the porosity distribution of the random porosity model in this study. Shown in Fig. 3, the solid line is the distribution of the general random variable ε of the normal distribution $N(0.5, 0.05^2)$ obtained from the Kinderman–Ramage procedure and the dashed line is the result of the theoretical normal distribution $N(0.5, 0.05^2)$. The deviation between both lines are small.

The permeability K, and inertia factor F are defined as [8]

$$K = \frac{\varepsilon^3 \overline{d}_p^2}{150(1-\varepsilon)^2} \quad (4)$$

$$F = \frac{1.75}{\sqrt{150\varepsilon^{1.5}}}. \quad (5)$$

The effective thermal conductivity of a porous medium k_e is a combination of the stagnant conductivity k_d and the thermal dispersion conductivity k_t [23], which simulates the transverse thermal dissipation. The relationship between k_e, k_d and k_t is then

$$k_e = k_d + k_t \quad (6)$$
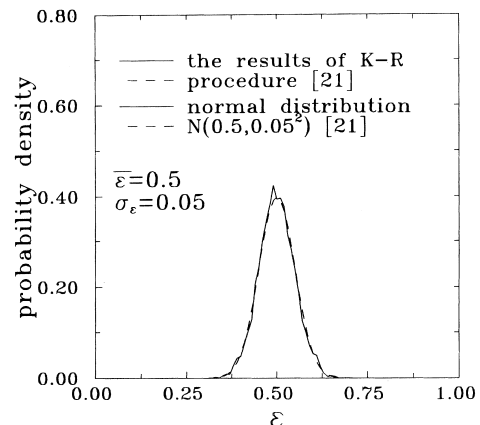
Fig. 3. The distributions of probability density of random variable ε of normal distribution $N(0.5, 0.05^2)$ generated by computer.

and k_d is defined as

$$\frac{k_d}{k_f} = 1 - \sqrt{1-\varepsilon} + \frac{2\Lambda\sqrt{1-\varepsilon}}{\Lambda - B_0} x \left[\frac{B_0\Lambda(\Lambda-1)}{(\Lambda-B_0)^2} \ln\left(\frac{\Lambda}{B_0}\right) \right.$$
$$\left. - \frac{B_0+1}{2} - \frac{\Lambda(B_0-1)}{\Lambda-B_0} \right] \quad (7)$$

where

$$\Lambda = \frac{k_s}{k_f} \quad (8)$$

$$B_0 = 1.25 \left(\frac{1-\varepsilon}{\varepsilon}\right)^{10/9} \quad (9)$$

and k_t is defined by Van Driest's wall function as

$$\frac{k_t}{k_f} = D_T Pr_f Re_p |\mathbf{u}_p| l \quad (10)$$

where D_T is an empirical constant, Re_p is the bead diameter based Reynolds number, defined as

$$Re_p = \frac{|\mathbf{u}_p|\overline{d_p}}{v_f} \quad (11)$$

where l is the Van Driest's wall function defined as

$$l = 1 - e^{-\Delta s/\omega\overline{d_p}} \quad (12)$$

and ω is an empirical constant.

Based on the above assumptions and with the following characteristic scales of b, $T_w - T_0$, ρv_0^2 and v_0, the governing equations, boundary conditions and geometry dimensions are normalized as follows:

(1) Governing equations of the external flow field

continuity equation

$$\frac{\partial U_f}{\partial X} + \frac{\partial V_f}{\partial Y} = 0 \quad (13)$$

X-momentum equation

$$U_f \frac{\partial U_f}{\partial X} + V_f \frac{\partial U_f}{\partial Y} = -\frac{\partial P_f}{\partial X} + \frac{1}{Re}\left(\frac{\partial^2 U_f}{\partial X^2} + \frac{\partial^2 U_f}{\partial Y^2}\right) \quad (14)$$

Y-momentum equation

$$U_f \frac{\partial V_f}{\partial X} + V_f \frac{\partial V_f}{\partial Y} = -\frac{\partial P_f}{\partial Y} + \frac{1}{Re}\left(\frac{\partial^2 V_f}{\partial X^2} + \frac{\partial^2 V_f}{\partial Y^2}\right) \quad (15)$$

energy equation

$$U_f \frac{\partial \theta_f}{\partial X} + V_f \frac{\partial \theta_f}{\partial Y} = \frac{1}{Re\,Pr_f}\left(\frac{\partial^2 \theta_f}{\partial X^2} + \frac{\partial^2 \theta_f}{\partial Y^2}\right). \quad (16)$$

(2) Governing equations of the internal flow field [7] for the porous block situation

continuity equation

$$\frac{\partial U_p}{\partial X} + \frac{\partial V_p}{\partial Y} = 0 \quad (17)$$

X-momentum equation

$$U_p \frac{\partial}{\partial X}\left(\frac{U_p}{\varepsilon}\right) + V_p \frac{\partial}{\partial Y}\left(\frac{U_p}{\varepsilon}\right) = -\frac{\partial P_p}{\partial X}$$
$$+ \frac{1}{Re}\left(\frac{\partial^2 U_p}{\partial X^2} + \frac{\partial^2 U_p}{\partial Y^2}\right) - \frac{1}{Re\,Da}\varepsilon U_p - \frac{F|\mathbf{U}_p|}{\sqrt{Da}}\varepsilon U_p \quad (18)$$

Y-momentum equation

$$U_p \frac{\partial}{\partial X}\left(\frac{V_p}{\varepsilon}\right) + V_p \frac{\partial}{\partial Y}\left(\frac{V_p}{\varepsilon}\right) = -\frac{\partial P_p}{\partial X}$$
$$+ \frac{1}{Re}\left(\frac{\partial^2 V_p}{\partial X^2} + \frac{\partial^2 V_p}{\partial Y^2}\right) - \frac{1}{Re\,Da}\varepsilon V_p - \frac{F|\mathbf{U}_p|}{\sqrt{Da}}\varepsilon V_p \quad (19)$$

energy equation

$$U_p \frac{\partial \theta_p}{\partial X} + V_p \frac{\partial \theta_p}{\partial Y} = \frac{\partial}{\partial X}\left(\frac{1}{Re\,Pr_p}\frac{\partial \theta_p}{\partial X}\right) + \frac{\partial}{\partial Y}\left(\frac{1}{Re\,Pr_p}\frac{\partial \theta_p}{\partial Y}\right). \quad (20)$$

(3) Boundary conditions

on surface AB (symmetrical line)

$$U_f = 0, \quad \frac{\partial V_f}{\partial X} = 0, \quad \frac{\partial \theta_f}{\partial X} = 0$$

$$U_p = 0, \quad \frac{\partial V_p}{\partial X} = 0, \quad \frac{\partial \theta_p}{\partial X} = 0 \quad (21)$$

on surface BC (heated region)

$$U_p = 0, \quad V_p = 0, \quad \theta_p = 1 \quad (22)$$

on surface CD (insulated region)

$$U_f = 0, \quad V_f = 0, \quad \frac{\partial \theta_f}{\partial Y} = 0 \quad (23)$$

on surface ED ($X \to \infty$)

$$\frac{\partial U_f}{\partial X} = 0, \quad \frac{\partial V_f}{\partial X} = 0, \quad \frac{\partial \theta_f}{\partial X} = 0 \quad (24)$$

on surface EF ($Y \to \infty$)

$$\frac{\partial U_f}{\partial Y} = 0, \quad \frac{\partial V_f}{\partial Y} = 0, \quad \frac{\partial \theta_f}{\partial Y} = 0 \quad (25)$$

on surface FG (wall)

$$U_f = 0, \quad V_f = 0, \quad \frac{\partial \theta_f}{\partial X} = 0 \quad (26)$$

on surface GA (jet inlet)

$$U_f = 0, \quad V_f = -1, \quad \theta_f = 0. \quad (27)$$

There are some interfacial conditions at the interfaces between the porous block and external flow field. These are the matching conditions of the horizontal and vertical velocities, normal and shear stresses, temperature, heat flux and pressure. However, these conditions will make the problem more complex. A simplified method suggested to solve these interfacial problems was discussed in the study of Hadim [12]. The interfacial conditions at the fluid/porous medium interface are

automatically satisfied [12] due to the Brinkman extension in the momentum equations for the porous medium.

3. Numerical method

The SIMPLEC algorithm [22] with TDMA solver [24] is used to solve the governing equations (13)–(20) for the flow and thermal fields. Equations (13)–(20) are first discretized into algebraic equations by using the control volume method [24] with a power-law scheme. The underrelaxation factor is 0.2 for both the fields of velocity and temperature. The conservation residues [22] of the equations of the momentum, energy and continuity and the relative errors of each variable are used to examine the convergence criteria which are defined as follows:

$$(\Sigma |\text{Residue of } \Phi \text{ equation}|^2_{\text{c.v.}})^{1/2} \leqslant 10^{-4},$$
$$\Phi = U, V, \theta, \text{and mass flow rate} \quad (28)$$

$$\frac{\max |\Phi^{n+1} - \Phi^n|}{\max |\Phi^{n+1}|} \leqslant 10^{-5}, \quad \Phi = U, V, P, \theta. \quad (29)$$

In order to reduce the computation time, a non-staggered mesh is used. The finer meshes are placed in both the interfacial region of the block and near the solid wall region. The meshes are then expanded outwards from the interfacial boundary and the solid wall with a scale ratio of 1.05. Also on the basis of the suggestions of Patankar [24], the harmonic mean formulation of thermophysical properties is used to avoid the effects of abrupt change of these properties across the interfacial region of the block and the external flow field on the computation accuracy.

The numerical method and accuracy are validated by Fu et al. [15, 16]. The comparison of the results of Miyarzaki and Silberman [25], which were derived by an analytical method for a case of a laminar slot jet impinging on a smooth wall, and the results of this study (solid line) are indicated in Fig. 4. The deviation between these two results is small.

The parameters which include the Reynolds number *Re*, block height *HP*, block length *LP* and mean porosity $\bar{\varepsilon}$, adopted in this study are tabulated in Table 1. The Darcy number *Da* listed in Table 1 is based on the mean porosity $\bar{\varepsilon}$. Since the porosity ε is not a constant in both the variable and random porosity models, hence the *Da* in each control volume is also a variable during the computation. For the *Re* = 450 cases, the whole dimensionless domain $X \times Y$ is 15.0×12.0 and the fully developed conditions at the outlet sections can be satisfied.

Table 2 shows the empirical constants used in the definitions of the porosity ε for the variable porosity model and the Van Driest's wall function *l* [equation (12)]. Where the D_T and ω are provided by Cheng and Hsu [23].
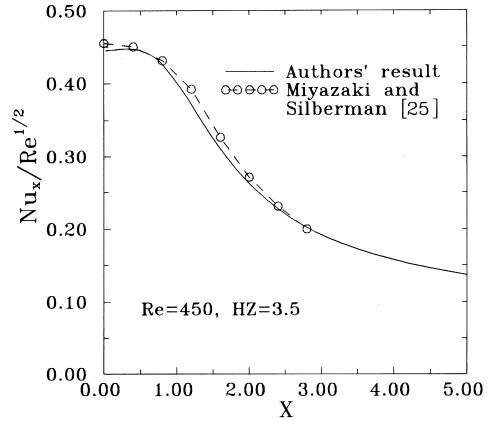
Fig. 4. The results of local Nusselt number distributions of jet impinging normally on smooth wall, compared with Miyazaki and Silberman [25].

Table 1
The main parameters

b (m)	Re	HP	HJ	LP	$\bar{\varepsilon}$	σ_ε	$\overline{d_p}$ (m)	Da	Pr
0.01	450	0.5	3.5	2	0.5	0.05	1.25E−3	5.208E−5	0.7

Table 2
The empirical constants for $\bar{\varepsilon} = 0.5$ ($\varepsilon_e = 0.307$)

r_1	r_2	D_T	ω
2.256	2	0.3	3.5

The results of grid tests are listed in Table 3, in order to gain more accurate results of the random porosity model, the 327×182 meshes are chosen in this study, and there are 76×68 meshes inside the porous block.

Table 3
Grid tests of porous block for $Re = 450$, $HP = 0.5$, $LP = 2$, $HJ = 3.5$, $\bar{\varepsilon} = 0.5$ and $Pr = 0.7$

Meshes of X	Meshes of Y	$\overline{Nu_p}$	Iterations
327	182	10.708	21 112
103	182	10.739	28 800
86	182	10.753	15 982
62	182	10.840	17 152
86	220	10.751	44 090
86	94	10.871	3189

4. Results and discussion

Without notice, $Re = 450$, $\bar{\varepsilon} = 0.5$, $\sigma_\varepsilon = 0.05$, $Pr = 0.7$, $HP = 0.5$, $LP = 2$ and $HJ = 3.5$ are fixed in the following situations.

Theoretically, there are infinite patterns generated by a random porosity model with a given mean porosity $\bar{\varepsilon}$ and standard deviation σ_ε. It is difficult to solve all of the patterns, therefore, only ten patterns with the same mean porosity $\bar{\varepsilon}$ ($=0.5$) are presented to investigate the effects of the random porosity model on the flow and thermal fields. The first three patterns (runs 1–3) have the same random variable ξ of the standard normal distribution but three different standard deviation σ_ε of 0.01, 0.05 and 0.1, respectively. The latter seven patterns (Runs 4–10) have the same standard deviation σ_ε ($=0.05$) with the different random porosity patterns.

The global porosity distribution maps and the near wall local porosity ε_x distributions along the X direction at $Y = 0.0015$ where it is the central position of the first control volume in Y direction during the computation, of the variable porosity model and two selected cases (Runs 2, 4) of the random porosity models are shown in Figs 5(a)–(f). In the global porosity distribution map, the total area is approximately divided into three main different porosity regions with different colors where the darker color represents the large porosity. For the variable porosity model, each color region has the same porosity interval of 0.22. However, for the random porosity models, the central region of the porosity index means the variation of the porosity to change from $\bar{\varepsilon} - \sigma_\varepsilon$ to $\bar{\varepsilon} + \sigma_\varepsilon$. In general, for the porous medium made of monosized and nonconsolidated beads, the pack between the solid beads and the solid wall is sparser than that between the beads and beads in the core region. Therefore, as shown in Figs 5(a) and (b) for the variable porosity model, the near wall local porosity ε_x is almost equal to unity, and the porosity in most regions varies from 0.32 to 0.54. Oppositely, for the random porosity model, as mentioned above the porosity distributions are not in order, then the pack between the beads and solid wall is no longer sparer than that of the other positions. Hence, for the random porosity models shown in Figs 5(c)–(f), the variation of porosity in the most region is from $\bar{\varepsilon} - \sigma_\varepsilon$ to $\bar{\varepsilon} + \sigma_\varepsilon$ and the variations of the near wall local porosity ε_x are drastic and disorder. Although the Runs 2 and 4 have the same mean porosity and standard deviation, the two cases have the different random variables, then the global porosity distributions and near wall local porosity ε_x distributions are different.

Shown in Figs 6(a)–(f), there are streamlines for the cases of the constant and variable porosity models and four selected cases (Runs 1–4) of the random porosity models, respectively. In order to illustrate the flow and thermal fields more clearly, the phenomena near the porous block are presented only. The dimensionless stream function ψ is defined as:
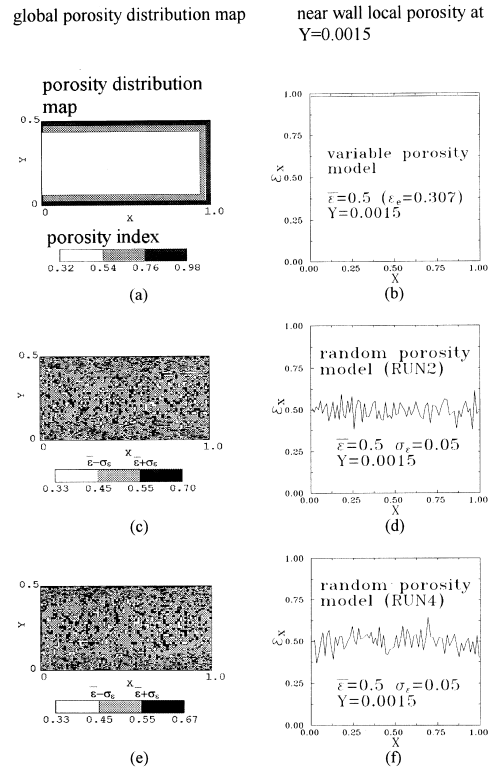
Fig. 5. Global porosity distribution map and near wall local porosity ε_x distribution at $Y = 0.0015$ along the X: (a) and (b) variable porosity model, $\bar{\varepsilon} = 0.5$ ($\varepsilon_e = 0.307$); (c) and (d) random porosity model, Run 2 ($\bar{\varepsilon} = 0.5$, $\sigma_\varepsilon = 0.05$); and (e) and (f) random porosity model, Run 4 ($\bar{\varepsilon} = 0.5$, $\sigma_\varepsilon = 0.05$).

$$U = \frac{\partial \psi}{\partial Y} \quad \text{and} \quad V = -\frac{\partial \psi}{\partial X}. \tag{30}$$

The fluids are issued from the jet inlet and impinge on the top surface of the porous block first. Due to the existence of the flow resistance inside the porous block, only a portion of the fluids can penetrate into the porous block. A circulation region neighboring to the right side of the block occurs. This flow pattern is disadvantageous to the heat transfer performance of the heated region. The flow pattern outside the porous block are similar for the six different cases. However, that the streamline of $\psi = 0.001$ of the variable porous model is close to the solid wall, which means that more fluids flow through the near wall region.

$\dot{m}_{p,in}$ and $\dot{m}_{p,out}$ are the flow rates of the fluids penetrating into and leaving from the porous block, respectively, and indicated in Table 4. Where $\dot{m}_0$ is the flow rate of the fluid issued from the jet inlet. The fluids penetrate into and leave from the porous block through the top and right side surfaces, respectively. The flow rate of the variable porosity model penetrating into the porous
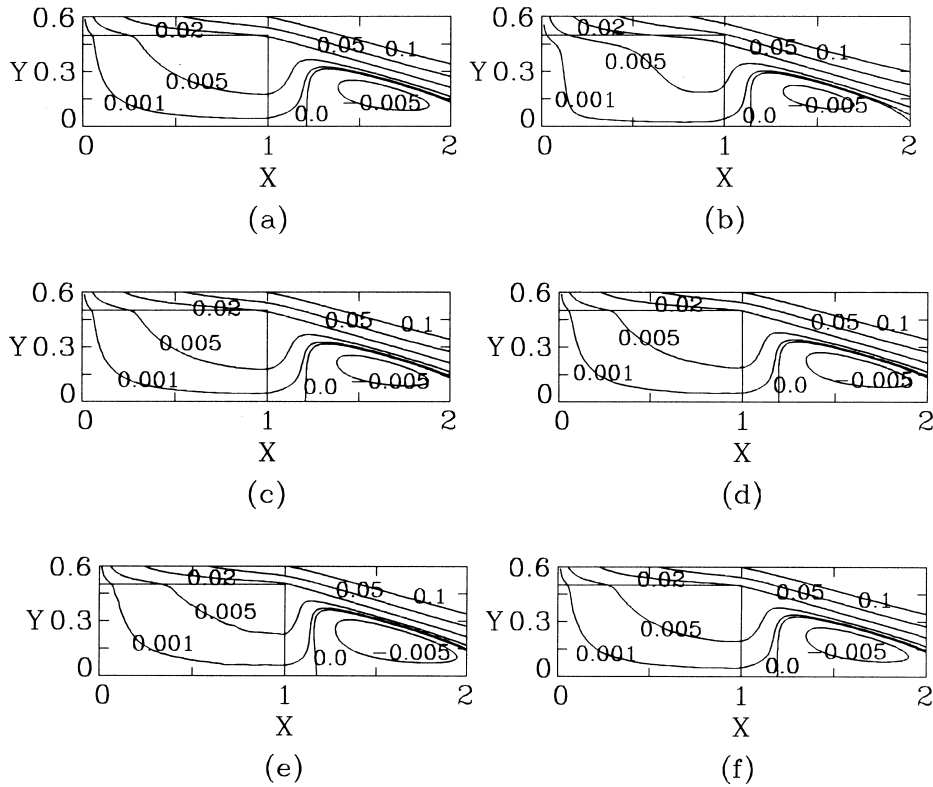
Fig. 6. Streamlines of different porosity models: (a) constant, (b) variable, (c) random, Run 1 ($\sigma_\varepsilon = 0.01$), (d) random, Run 2 ($\sigma_\varepsilon = 0.05$), (e) random, Run 3 ($\sigma_\varepsilon = 0.1$) and (f) random, Run 4 ($\sigma_\varepsilon = 0.05$).

Table 4
Ratio of flow rate ($\dot{m}_p$) penetrating into the porous block to that of jet inlet ($\dot{m}_0$)

Porosity model		Ratio of flow rate			
		Top surface		Right side surface	
		$\dot{m}_{p,in}/\dot{m}_0$	$\dot{m}_{p,out}/\dot{m}$	$\dot{m}_{p,in}/\dot{m}_0$	$\dot{m}_{p,out}/\dot{m}$
Constant		0.0450	0	0	0.0450
Variable		0.0935	0	0	0.0935
Random	Run 1	0.0448	0	0	0.0448
	Run 2	0.0416	0	0	0.0416
	Run 3	0.0338	0	0	0.0338
	Run 4	0.0421	0	0	0.0421
	Run 5	0.0417	0	0	0.0417
	Run 6	0.0427	0	0	0.0427
	Run 7	0.0434	0	0	0.0434
	Run 8	0.0415	0	0	0.0415
	Run 9	0.0423	0	0	0.0423
	Run 10	0.0417	0	0	0.0417

block is almost two times of those of the other two models. In addition, the flow rate of the constant porosity model is larger than those of the random porosity models. As for the flow rates of the first three cases of the random porosity models (Runs 1, 2, and 3), the smaller the standard deviation σ_ε, the larger the flow rate becomes. The reason may be suggested as that the more uniform porosity distribution is, the more fluids penetrate through the porous medium under $\bar{\varepsilon} = 0.5$ situation.

The local velocity U distribution in the near wall region along the Y direction at four different X positions, $X = 0.25, 0.5, 0.75$ and 0.95 are illustrated in Figs 7(a)–(d), respectively. Only the data of the Run 2 are selected from the cases of all random porosity models and indicated in the figures. Since the porosity varies casually, the local velocity U of the random porosity model presents a jagged profile and the channeling effect does not appear. In general, the distribution of local U velocities of the random porosity model are similar to that of the constant porosity model, the reason is that most of the values of the local porosity vary from $\bar{\varepsilon} - 2\sigma_\varepsilon$ to $\bar{\varepsilon} + 2\sigma_\varepsilon$, which occupies almost 95% of the full porosity distribution.
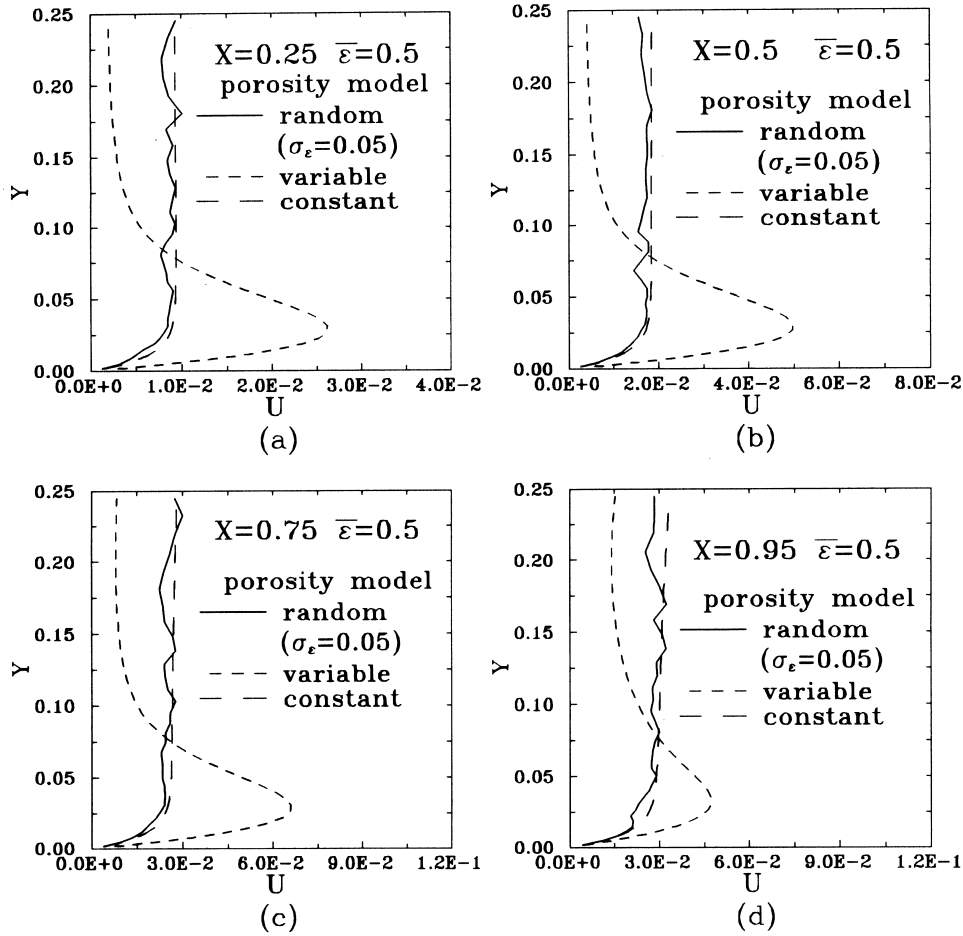
Fig. 7. The distributions of velocity U along the Y direction at (a) $X = 0.25$, (b) $X = 0.5$, (c) $X = 0.75$ and (d) $X = 0.95$.

When the value of σ_ε is small, the value of $\bar{\varepsilon} - 2\sigma$ is close to that of $\bar{\varepsilon} + 2\sigma_\varepsilon$.

For the variable porosity model, the maximum value of the local velocity U increases first as X increases and decreases after $X = 0,75$. However, a different trend exists for the constant and random porosity models, the maximum (or bulk) velocity U gradually increases with the increase of the X. The velocity gradient $(\mathrm{d}U/\mathrm{d}Y)$ in the near wall region of the variable porosity model is larger than those of the other models.

The isotherms of the cases of the constant and variable porosity models and four selected cases (Runs 1–4) of the random porosity models are illustrated in Figs 8(a)–(f), respectively. Like the results of the streamlines shown in Figs 6(a)–(f), the isotherm distributions of the four selected cases of the random porosity models are similar to that of the constant porosity model. That the isotherms are concentrated near the heated plate in the variable

porosity model is different from those of the other two models.

Shown in Figs 9(a)–(d) are the distributions of the local Nusselt number Nu_x of the variable and constant porosity models and four selected cases (Runs 1–4) of the random porosity models. Where the local Nusselt number Nu_x is defined as

$$Nu_x = \frac{h_x b}{k_f} = -\frac{k_e}{k_f} \frac{\partial \theta}{\partial Y}\bigg|_{Y=0}. \tag{31}$$

The higher the standard deviation σ_ε is, the larger the fluctuation of the porosity distribution becomes. Then the fluctuation of the local Nusselt number Nu_x distribution along the heated plate for the random porosity model increases as the standard deviation σ_ε increases as shown in Figs 9(a)–(c). Inversely, the variation of the distribution of the Nu_x of the smaller value of standard deviation σ_ε, e.g. $\sigma_\varepsilon = 0.01$ (Run 1), follows that of the
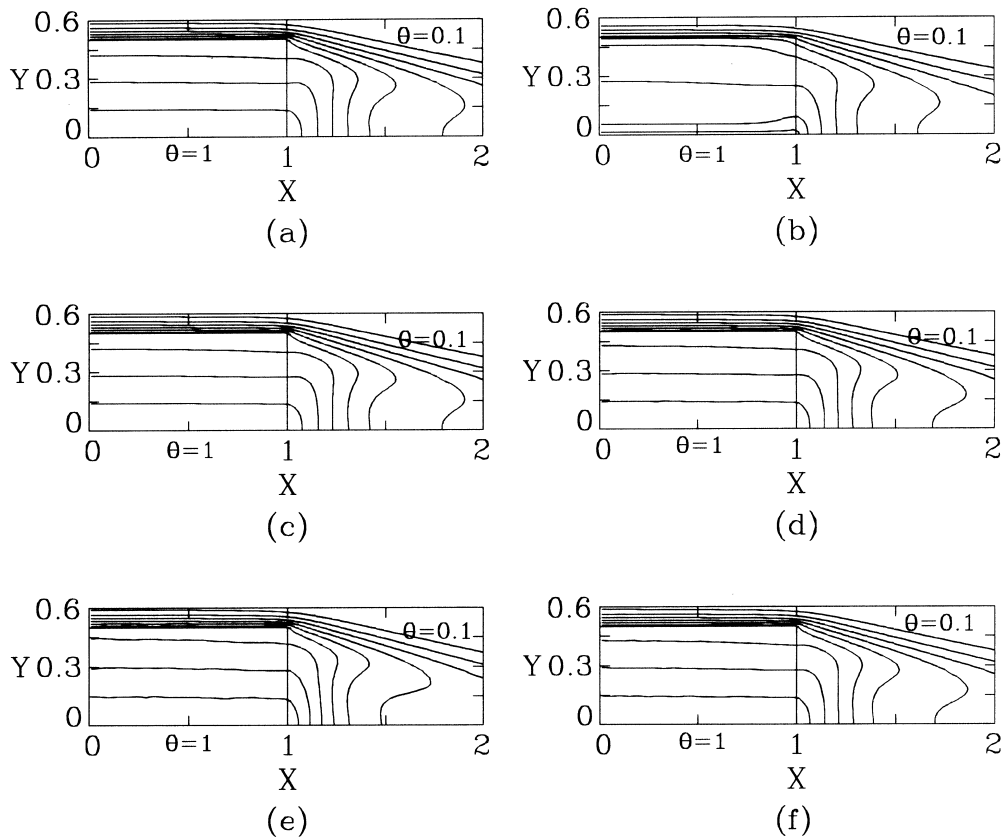
Fig. 8. Isotherms of different porosity models: (a) constant, (b) variable, (c) random, Run 1 ($\sigma_\varepsilon = 0.01$), (d) random, Run 2 ($\sigma_\varepsilon = 0.05$), (e) random, Run 3 ($\sigma_\varepsilon = 0.1$) and (f) random, Run 4 ($\sigma_\varepsilon = 0.05$).

constant porosity model with slight fluctuations. For the cases of Runs 2 and 4, due to the different random variables, the results of Runs 2 and 4 are different. Consequently, it is possible to obtain different heat transfer performances of the porous blocks with the same mean porosity and standard deviation. For the variable porosity model, the local Nusselt number near the right side wall of the porous block decreases with the increase of the X, however, the Nu_x increases in this region for both the constant and random porosity models. The phenomenon is induced by the development of the local U velocity along the X mentioned in Figs 7(a)–(d).

The effect of the near wall local porosity ε_x defined earlier at $Y = 0.0015$ on the local Nusselt number Nu_x for all eight cases of $\bar\varepsilon = 0.5$, $\sigma_\varepsilon = 0.05$ (runs 2, 4–10) are indicated in Fig. 10. In essence, the larger the ε_x, the effective thermal conductivity k_e is smaller, therefore, the relationship between the Nu_x and ε_x is a negative correlation as shown in Fig. 10. The heat transfer mechanism between the porous medium and the heated plate is the combination of conductive and convective heat transfer. Since the smaller porosity means that more solid phase

exists which contributes the conductive path to the heat transfer and the inference that the convective heat transfer herein is not a role may be drawn. Consequently, in order to enhance the thermal performance of the porous medium, the porosity near the heated plate should be smaller to cause the conductive heat transfer to be dominant.

In order to validate the above inference, the heat transfer rate of an artificial random porosity case (artificial random porosity model, Run 11) is examined. The values of the porosity ε of the artificial random porosity model are sorted out from the random porosity model of the Run 2 ($\bar\varepsilon = 0.5$ and $\sigma_\varepsilon = 0.05$). The porosity distribution of this model is reordered and arranged by the following rules shown in Fig. 11. The most dense porosity is arranged at the control volume 1 (the left most of the first row), as the value of the X increases the porosity becomes sparse. The porosity of the control volume 77 (the left most of the second row) is right behind the porosity of the control volume 76 (the right most of the first row) in the order of sparsity, and as the value of the X increases, the porosity becomes more sparse as the row
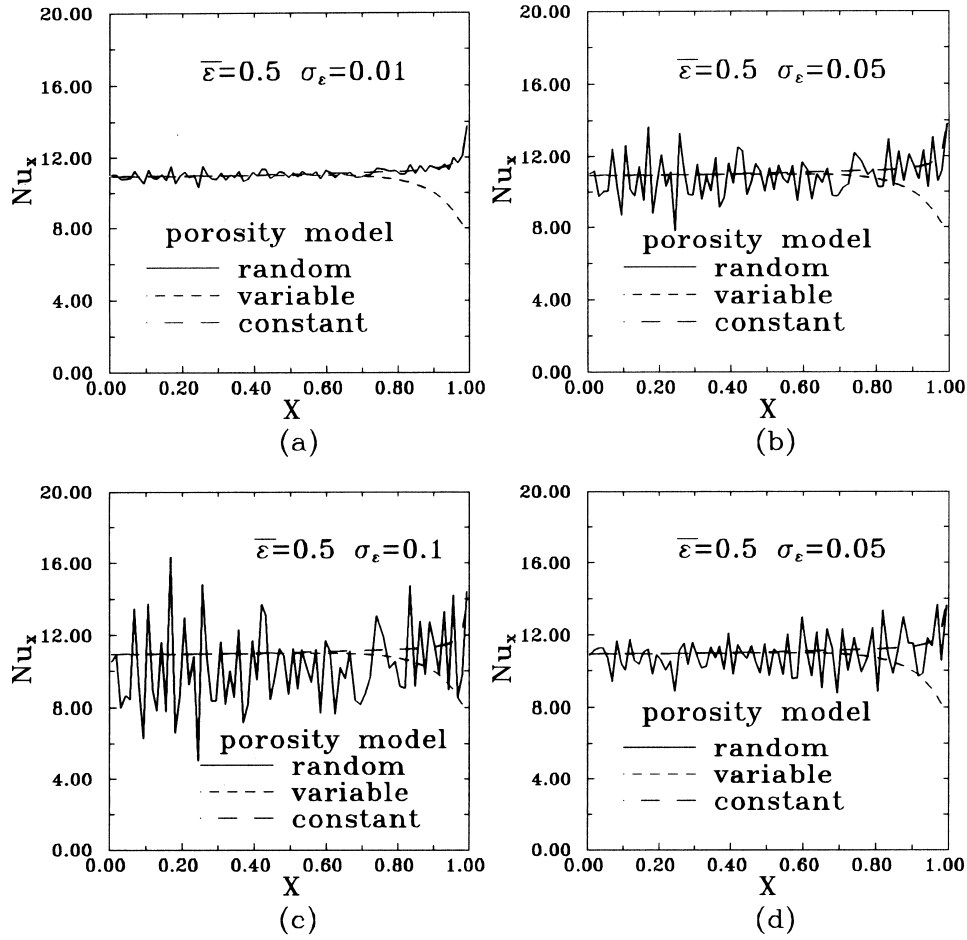
Fig. 9. The distributions of local Nusselt number Nu_x for four selected cases of the random porosity models: (a) Run 1 ($\sigma_\varepsilon = 0.01$), (b) Run 2 ($\sigma_\varepsilon = 0.05$), (c) Run 3 ($\sigma_\varepsilon = 0.1$) and (d) run 4 ($\sigma_\varepsilon = 0.05$).
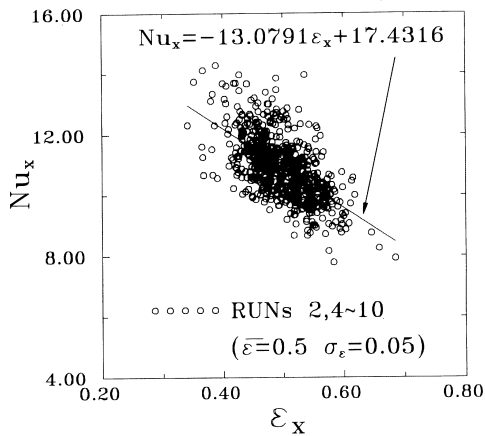
Fig. 10. The relationship between the near wall local porosity ε_x and local Nusselt number Nu_x.
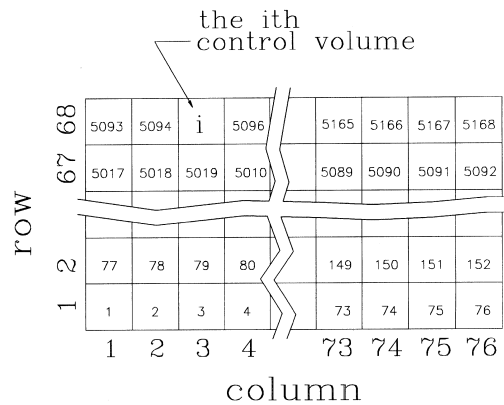
Fig. 11. The array of the porosity in the artificial random porosity model.

1. Follow the same rule until the last row, and the most sparse porosity is arranged at the right upper corner. The local Nusselt number Nu_x distributions along the X direction are shown in Fig. 12. The results of the random porosity model are the average values of the total eight cases (Runs 2, 4–10) at each X position. The local Nusselt number Nu_x of the artificial random porosity model is larger than those of the other three models. The results are in agreement with the above inference.

5. Conclusions

A flow and thermal field of a porous block with random porosity distribution under a laminar slot impinging jet are investigated numerically. The effects of the random porosity model on flow and thermal fields are examined and compared with those of the constant and variable porosity models. The results can be summarized as follows:

(1) The local Nusselt number distribution of the random porosity model are more similar to those of the constant porosity model than those of the variable porosity model with the smaller standard deviation. However, as the value of the standard deviation is larger, the fluctuation of the local Nusselt number is drastic and apparently different from those of the other two models.
(2) The relationship between the local Nusselt number Nu_x and the near wall local porosity ε_x is a negative correlation.
(3) In order to enhance the thermal performance of the porous medium, the porosity near the heated plate should be smaller to make the conductive heat transfer dominant.
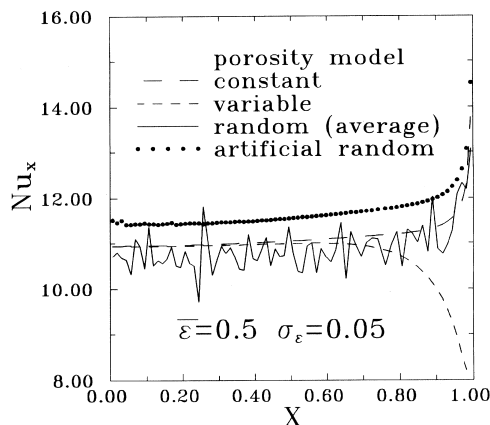
Fig. 12. The local Nusselt number Nu_x distributions of four different porosity models.

Appendix: the Kinderman–Ramage procedure

The Kinderman–Ramage procedure uses a mixture of distributions, λ_1, λ_2, and λ_3, to generate a standard random variable ξ, where the λ_1, λ_2, and λ_3 are three computer generated pseudo-random variables with double precision, such that $0.0 < \lambda_1, \lambda_2, \lambda_3 < 1.0$. The algorithm of the Kinderman–Ramage procedure is as follows [21]:

Step 1. Generate λ_1. If $\lambda_1 < 0.884070402298758$, generate λ_2 and deliver

$$\xi = a(1.13113163544180\lambda_1 + \lambda_2) - 1$$

where $a = 2.216035867166471$. Then go to Step 10.

Step 2. If $\lambda_1 < 0.973310954173898$, go to Step 4.

Step 3. Generate λ_2 and λ_3 until

$$\lambda_2^2 < a^2(a^2 - 2\ln(\lambda_3))^{-1},$$

then if $\lambda_1 < 0.9866554770869489$ then deliver

$$\xi = (a^2 - 2\ln(\lambda_3))^{1/2}$$

else deliver $\xi = -(a^2 - 2\ln(\lambda_3))^{1/2}$. Then go to Step 10.

Step 4. If $\lambda_1 < 0.958720824790463$, go to Step 6.

Step 5. Generate λ_2 and λ_3. Set

$$t = a - [0.630834801921960 \min(\lambda_2, \lambda_3)].$$

If $\max(\lambda_2, \lambda_3) \leqslant 0.755591531667601$, go to Step 9.
If $0.034340503750111 (|\lambda_2 - \lambda_3|) \leqslant g(t)$, go to Step 9; otherwise repeat Step 5.
where
$$g(t) = \phi(t) - 0.18002519106563 + (a - |t|) \text{ for } |t| < a$$
and
$$\phi(t) = 1/\sqrt{2\pi}\, e^{-t^2/2} \text{ (normal density function)}$$

Step 6. If $\lambda_1 < 0.911312780288703$, go to Step 8.

Step 7. Generate λ_2 and λ_3. Set

$$t = 0.479727404222441 + [1.105473661022070 \min(\lambda_2, \lambda_3)]$$

If $\max(\lambda_2, \lambda_3) \leqslant 0.872834976671790$, go to Step 9.
If $0.049264496373128 (|\lambda_2 - \lambda_3|) \leqslant g(t)$, go to Step 9; otherwise repeat Step 7.

Step 8. Generate λ_2 and λ_3. Set

$$t = 0.479727404222441 - [0.595507138015940 \min(\lambda_2, \lambda_3)]$$

If $\max(\lambda_2, \lambda_3) \leqslant 0.80557792443817$, go to Step 9; otherwise repeat Step 8.

Step 9. If $\lambda_2 < \lambda_3$, deliver $\xi = t$; otherwise deliver $\xi = -t$. Then go to Step 10.

Step 10. Transform the standard random variable ξ into the random variable ε with given $\bar{\varepsilon}$ and σ_ε. The relationship between ξ and ε is

$$\varepsilon = \bar{\varepsilon} + \xi \times \sigma_\varepsilon.$$

References

[1] L.H.S. Roblee, R.M. Baird, J.W. Tiern, Radial porosity variations in packed beds, American Institute of Chemical Engineers Journal 4 (1958) 460–464.

[2] R.F. Benenati, C.B. Brosilow, Void fraction distribution in packed beds, American Institute of Chemical Engineers Journal 8 (1962) 359–361.

[3] C.E. Schwartz, J.M. Smith, Flow distribution in packed beds, Industrial and Engineering Chemistry 45 (1952) 1209–1218.

[4] C.E. Schwartz, K.B. Bischoff, Thermal and material transport in nonisothermal packed beds, American Institute of Chemical Engineers Journal 15 (1969) 597–604.

[5] P. Cheng, A. Chowdhury, C.T. Hsu, Forced convection in packed tubes and channels with variable porosity and thermal dispersion effects, in: S. Kakaç et al. (Eds.), Convective Heat Mass Transfer in Porous Media, 1991, pp. 625–653.

[6] K. Vafai, C.L. Tien, Boundary and inertia effects on flow and heat transfer in porous media, International Journal of Heat and Mass Transfer 24 (1981) 195–203.

[7] C.T. Hsu, P. Cheng, Thermal dissipation in a porous medium, International Journal of Heat and Mass Transfer 33 (1990) 1587–1597.

[8] K. Vafai, Convective flow and heat transfer in variable-porosity media, Journal of Fluid Mechanics 147 (1984) 233–259.

[9] A. Amiri, K. Vafai, Analysis of dispersion effects and non-thermal equilibrium, non-Darcian, variable porosity incompressible flow through porous media, International Journal of Heat and Mass Transfer 37 (1994) 939–954.

[10] M. Kaviany, Laminar flow through a porous channel bounded by isothermal parallel plates, International Journal of Heat and Mass Transfer 28 (1985) 851–858.

[11] P. Cheng, H. Zhu, Effects of radial thermal dissipation of fully-developed forced convection in cylindrical packed tubes, International Journal of Heat and Mass Transfer 30 (1987) 2373–2383.

[12] A. Hadim, Forced convection in a porous channel with localized heat sources, Journal of Heat Transfer 116 (1994) 465–472.

[13] M.L. Hunt, C.L. Tien, Effects of thermal dissipation on forced convection in fibrous media, International Journal of Heat and Mass Transfer 31 (1988) 301–309.

[14] W.S. Fu, H.C. Huang, W.Y. Liou, Thermal enhancement in laminar channel flow with a porous block, International Journal of Heat and Mass Transfer 39 (1996) 2165–2175.

[15] W.S. Fu, H.C. Huang, Thermal performances of different shape porous blocks under an impinging jet, International Journal of Heat and Mass Transfer 40 (1997) 2261–2272.

[16] W.S. Fu, H.C. Huang, Appropriate sizes of porous and solid blocks for heat transfer under an impinging jet, Journal of the Chinese Institute of Engineers 20 (1997) 159–169.

[17] J.G. Georgiads, I. Catton, Stochastic modeling of unidirectional fluid transport in uniform and random packed beds, The Physics of Fluids 30 (1987) 1017–1022.

[18] I. Catton, J.G. Georgiads, P. Adnani, The impact of nonlinear convective processes on transport phenomena in porous media, Proceedings of 1988 National Heat Transfer Conference, Vol. 1, ASME HTD-96, Houston, 1988, pp. 767–777.

[19] J.G. Georgiads, Effect of randomness on heat and mass transfer in porous media, in: S. Kakaç et al. (Eds.), Convective Heat Mass Transfer in Porous Media, 1991, pp. 499–524.

[20] A. Saito, S. Okawa, T. Suzuki, H. Maeda, Calculation of permeability of porous media using direct simulation Monte Carlo method (effect of porosity and void distribution on permeability), Proceedings of ASME/JSME Thermal Engineering Joint Conference, Vol. 3, Maui, 1995, pp. 297–304.

[21] W. J. Kennedy Jr, J.E. Gentle, Statistical Computing, Marcel Dekker, New York, 1980.

[22] J.P. Van Doormaal, G.D. Raithby, Enhancements of the SIMPLE method for predicting incompressible fluid flows, Numerical Heat Transfer 7 (1984) 147–163.

[23] P. Cheng, C.T. Hsu, Applications of Van Driest's mixing length theory to transverse thermal dissipation in a packed-bed with boundary walls, International Communication in Heat and Mass Transfer 13 (1986) 613–625.

[24] S.V. Pantankar, Numerical Heat Transfer and Fluid Flows, Hemisphere. Washington D.C., 1980.

[25] H. Miyazaki, E. Silberman, Flow and heat transfer on a flat plate normal to a two-dimensional laminar jet issuing from a nozzle of finite height, International Journal of Heat and Mass Transfer 15 (1972) 2097–2107.